Controlled Hydrogel Fiber Formation: The Unique Case of Hexaphenylbenzene-Poly(ethylene glycol) Amphiphiles

Katrin Wunderlich, Antje Larsen, John Marakis, George Fytas, Markus Klapper,* and Klaus Müllen*

Fiber formation in nature occurs not only at surfaces but also in bulk from large molecules such as collagen. The relation between water and biological macromolecules is one of the most important phenomena of all life processes. Connective tissue, for example, depends upon the association with water for the unique and specific mechanical properties. Here water is an important component of both the collagen fibers and the polysaccharide gel matrix which comprises the highly organized composite structure (structural, bound and free water).[1] Swelling yields hydrogel fibers, wherein the overall structure is not destroyed by water uptake. This example shows that nature is able to activate weak intermolecular interactions (hydrogen bonds, van der Waals forces) to control fiber formation.[2] The control of the interaction strength is decisive for the formation of biological fibers by self-assembly processes.[3] The strength should be high enough to form stable structures under physiological (aqueous) conditions but also sufficiently low to yield defined thermodynamic equilibrium structures.

In fiber formation processes, chemists use either physical methods such as extruding,[4] microfluidic processes,[5] electrospinning[6] or also molecular self-assembly, i.e., formation of discrete architectures from molecules via intermolecular forces, thereby competing with nature.[7–11] However, a dense packing inside the core and the shell is always assumed and possible partition of water was ignored. Hydrogel fibers can be formed by synthetic methods as well, however, they require a chemical crosslinking. For example, extruded fibers of poly(vinyl alcohol) and poly(acrylic acid) can be converted to bundles of hydrogel fibers after a crosslinking by ester formation upon heating.[12,13]

We attempt to mimic the concepts of nature to form synthetic hydrogel fibers via self-assembly by carefully adjusting the molecular interactions of different amphiphiles. In the present study, hexaphenylbenzene (HPB) was chosen as the large hydrophobic section and PEG as hydrophilic part of the amphiphile on the account of their large antagonistic forces.[14] Smaller amphiphiles like sodium dodecyl sulfate or lutensols with high critical micelle concentration (cmc) form only small aggregates (micelles) while amphiphilic block copolymers yield kinetically arrested non-equilibrium structures.[15,16] Additionally, we favored the propeller-like HPB over the corresponding dehydrogenated disk-like hexa-*peri*-hexabenzocoronene (HBC) as hydrophobic building block. The latter case is already known for forming extended columns in solution, however, due to the strong π–π interactions between the extended polyaromatic units[17] a thermodynamic control of the aggregation process cannot be guaranteed. Furthermore, the shape of the PEG functionalized HPB can be easily changed by varying the number and chain length of the solubilizing group without altering the fraction of the solubilizing PEG units. We define the shape on Israelachvili's packing parameter.[9] Our definition is based on the different shapes of the molecules with a random coil of PEG in which we assume that the cone becomes broader with more arms at the same position (schematic representation of **Figure 1**).[18]

In this concept, we anticipate that, depending on the molecular shape and the length of the PEG chains (i.e., density of the hydrophilic group in the periphery of HPB, Figure 1), space filling will control water uptake by the formed hydrogel fibers. In particular, we have synthesized amphiphilic compounds based on HPB with two different PEG substitution patterns and investigated their self-assembly behavior in water. The characterization of the resulting supramolecular assemblies imposes additional challenges considering their complexity (size, shape and dynamic nature) and the inevitable extremely dilute conditions, necessary to avoid interactions between them. Performing dynamic polarized and depolarized light scattering, we assessed both the form factor and the two transport (translation, rotation) coefficients of the assemblies necessary to uniquely reveal their complex structures. Based on the characteristic parameters (the number of molecules within the fibers N_S, length L_w, diameter d, length density M/L), the supramolecular structure can be represented by bundles of fibers. Their size and water content relate to the structure and amphiphilicity of **1** and **2**; both vary with the number and length of the PEG chains (Figure 1).

K. Wunderlich, Dr. M. Klapper, Prof. Dr. K. Müllen
Max Planck Institute for Polymer Research
Ackermannweg 10 55128, Mainz, Germany
E-mail: klapper@mpip-mainz.mpg.de
A. Larsen, J. Marakis, Prof. Dr. G. Fytas
Department of Materials Science and Technology
University of Crete and F.O.R.T.H.
P.O. Box 1527, 71110, Heraklion, Greece
E-mail: fytas@mpip-mainz.mpg.de

DOI: 10.1002/smll.201302832

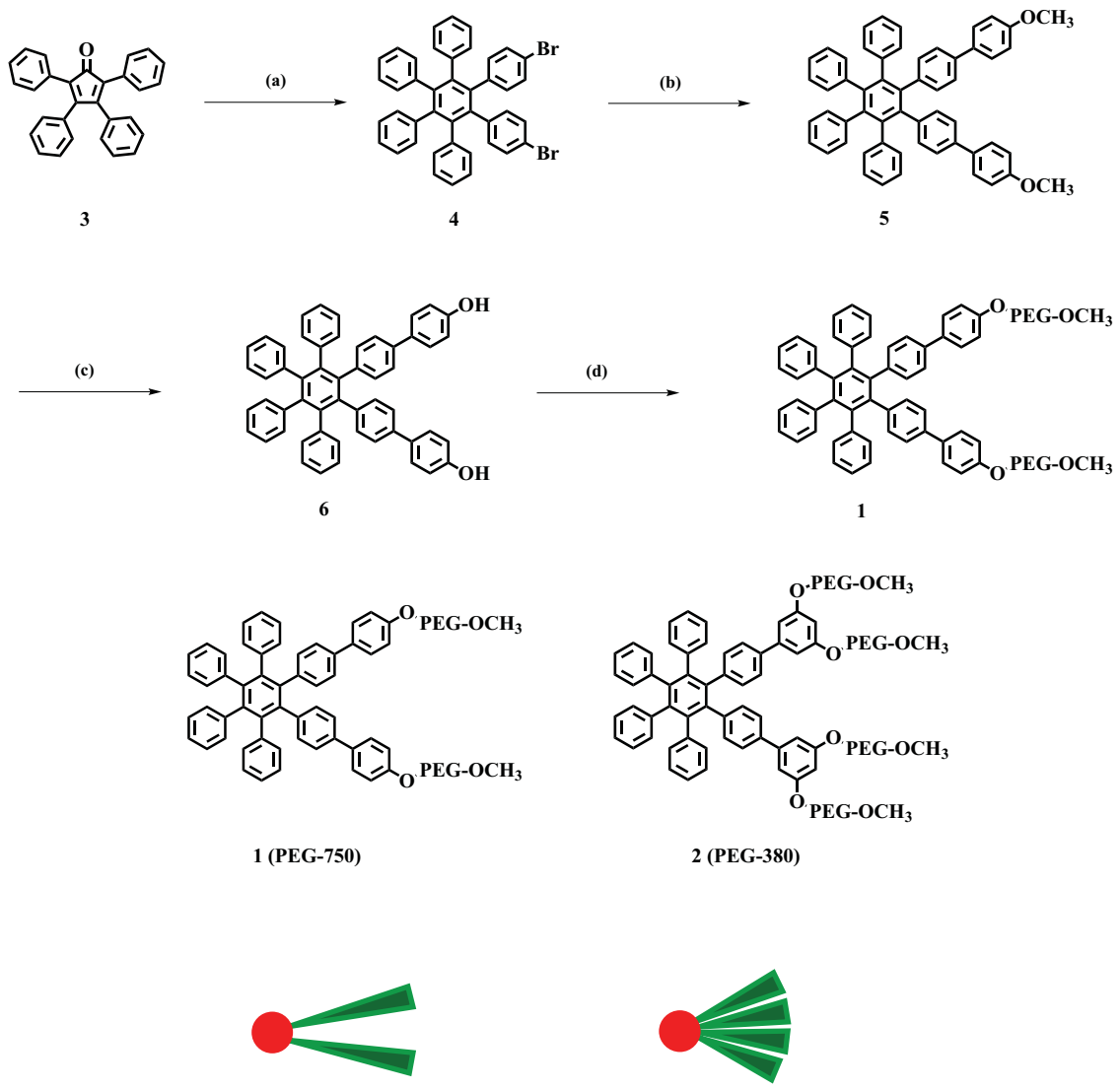

Figure 1. Synthetic scheme for **1**. (a) 1,2-bis(4-bromophenyl)ethyne, diphenyl ether, microwave: 220 °C, 300 W, 12 h (45%); (b) (4-methoxyphenyl) boronic acid, $Pd(OAc)_2$, Cs_2CO_3, DABCO, DMF, 80 °C, 3d (65%); (c) BBr_3, DCM, 0 °C to rt (84%); (d) CH_3O-PEG-Br, KOH, THF, reflux, 18 h. Molecular structure and the schematic representation of **1** (**PEG-750**) and **2** (**PEG-380**).

We synthesized the title compounds (Figure 1) through a Diels-Alder reaction with subsequent CO extrusion of 2,3,4,5-tetraphenylcyclopenta-2,4-dienone (**3**) and 1,2-bis(4-bromophenyl)ethyne led to 4,4″-dibromo-3′,4′,5′,6′-tetraphenyl-1,1′:2′,1″-terphenyl (**4**). 4,4′′′′-Dimethoxy-3″,4″,5″,6″-tetraphenyl-1,1′:4′,1″:2″,1‴:4‴,1′′′′-quinquephenyl (**5**) was prepared by palladium-catalyzed Suzuki coupling reaction with 4-methoxyphenyl boronic acid. The following deprotection of the methoxyphenyl groups and etherification of HPB containing two hydroxyphenyl groups (**6**) with α-methoxy-ω-bromo-PEG (PEG: M_n = 750 g mol^{-1}) gave **1** (Figure 1); while **2** was synthesized under similar conditions.

The self-assembly behavior of hexaphenylbenzene containing PEG molecules with different architecture (**1** and **2**) was explored in aqueous solution by cryo-TEM. For the aqueous solution of **1** at 30.7g L^{-1}, long self-assembled structures are observed with a worm-like structure (**Figure 2**). The length of worm-like micelles of sample **1** displays in the range of ~5 and ~350 nm with a diameter of ~3 nm.

The cmc values of these samples as estimated from the change of the surface tension with increasing concentration are indeed very low. Sample **2** possesses a cmc value of 0.002 g L^{-1} which is even lower than for sample **1** (Figure S1, Supporting Information). The latter seems to display two crossover concentrations between 0.003 and 0.01 g L^{-1}. Therefore, the cryo-TEM image (Figure 2), obtained at concentrations (~30 g L^{-1}) several orders of magnitude above cmc, might render any prediction of the structures at much lower concentrations (near cmc) ambiguous. The surface tension profile of **2** is similar to the surface tension profile of conventional ionic surfactant such as sodium dodecyl sulfate (SDS).[19] The measured cmc values are clearly lower than the cmc of ionic surfactants which assume values in the range of g L^{-1} (cmc_{SDS} = 2.65 g L^{-1}).[20] Very small cmc, comparable to the value of **2**, occur for high molecular weight block copolymers. However,

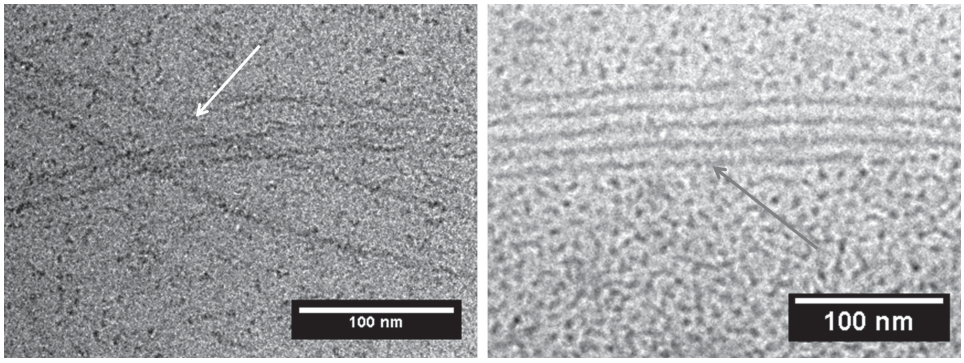

Figure 2. Cryo-TEM micrograph of **1** in aqueous solution at 30.7 g L^{-1}. The white arrow shows worm-like structures and the black arrow shows a bundle of fibers.

these values are obtained from air/water interface measurements and might deviate for the bulk solution. The performed dynamic light scattering experiment at different concentrations utilized the photon correlation spectroscopy (PCS) technique. This method, having the necessary spatiotemporal resolution, has reconciled all available structural information of the self-assembly behavior of **1** and **2**.

We have initiated the PCS experiment with a concentration of 1.7 g L^{-1} that is between cmc and the concentration used for the cryo-TEM images. We first examined aqueous solutions of **1** prepared at 20 °C and also recorded the experimental relaxation function $C_{vv}(q,t)$ also at 20 °C at a high scattering wave vector $q = 0.03$ nm^{-1} corresponding to a probing length of about 200 nm (open squares in Figure S2). Dynamics of the order of 100 μs cannot be rationalized by the small size of the structures of **1** and **2** and clearly implies formation of supramolecular assemblies. The broad shape of the relaxation function describing the diffusion dynamics of the moieties present in the solution was analyzed by ILT (Equation 1a, SI). Two populations of assemblies are revealed which unexpectedly change with annealing at 20 °C over a period of about weeks. To speed up this equilibration procedure and warrant time invariant structures, we have annealed the solutions at 50 °C for about 3 h with subsequent slow cooling to 20 °C.

The recorded $C_{vv}(q,t)$ (blue solid rhombi) is different from the relaxation function before the particular annealing protocol was employed as both peaks of ILT shift to shorter times with heating and the stronger impact is on the amplitude and position of the slow process. This peculiar metastability effect is not observed for the aqueous solutions of **2** at similar concentration (inset of Figure S2). The depicted $C_{VV}(q,t)$ recorded as-dissolved (black open squares) and after annealing at 50 °C (blue open rhombi) display experimentally the same shape as it is reflected more in the corresponding ILT profiles. The origin of kinetically trapped structures in relatively dilute concentrations of the present amphiphiles due to the formation of thermodynamically unfavorable configurations is unclear and needs further investigation. For the elucidation of the formed structures, however, it suffices to know the pathway towards equilibrium of self-assembled structures.

The second unexpected observation relates to the very low overlap concentration c* above which interactions between the supramolecular assemblies in the aqueous solutions become important; their structural characterization is meaningful at c<c*. The reduced Rayleigh ratio $R_{VV}(q\rightarrow0)/c$ for the samples **1** and **2** obtained from the extrapolation of the q-dependent $R_{VV}(q)$ at $q = 0$ (**Figure 3**) represents the reciprocal of the osmotic pressure of the solutions, and hence its concentration dependence significantly reflects interactions between solutes.[21] This diagram identifies two regimes with a crossover c* roughly around 0.1 g L^{-1} for **1** with the dilute regime, identified by $R_{VV}(q\rightarrow0)\sim c$, below this concentration. Above c* two relaxation processes are present in $C_{VV}(q,t)$ (Figure S2) with intensity contributions (circles and squares) (Figure 3); this crossover concentration is larger than the two values for **1** (Figure S1 and arrows in Figure 3). Above about this c*, two processes are also observed in the $C_{VV}(q,t)$ for **2** (Figure S3) but a c-independent $R_{VV}(q\rightarrow0)/c$ is reached at much lower concentrations (<0.002 g L^{-1}) in agreement with its cmc value (red arrow in Figure 3). However, the limiting $R_{VV}(q\rightarrow0)/c$ values for both **1** and **2** do not correspond to the molecular species (Figure 1) but to much larger structures as indicated

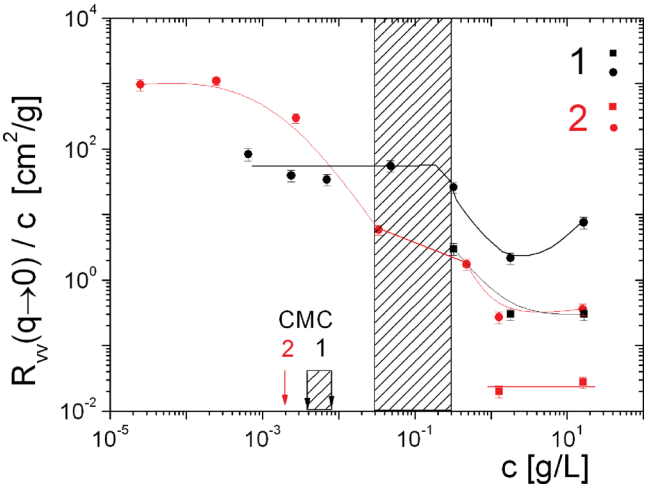

Figure 3. Reduced absolute scattering intensity $R_{vv}(q\rightarrow0)/c$ is shown as function of concentration, c, at 20 °C for **1** and **2.** The shaded area indicates a crossover to semidilute regime in which two relaxation processes are resolved in $C_{vv}(q,t)$. Circles and squares denote the R_{vv} intensities associated with the main and fast processes. The two arrows are for the CMC values from Figure S1.

NANO MICRO small

by the estimated molecular weight $M_w = R_{VV}$ (q→0)/Hc. Using for the contrast factor $H = [2\pi n(dn/dc)]^2/(N_A \lambda^4) = 5.5\cdot10^{-7}$ cm^2 mol g^{-2}, with N_A being the Avogadro number, M_w amounts to $1.3\cdot10^8$ g mol^{-1} and $1.8\cdot10^9$ g mol^{-1} for the assemblies in **1** and **2** aqueous solutions at c ~0.001 g L^{-1} below cmc, respectively. The latter obtained from surface tension measurements (Figure S1) does not signify a transition to molecular species and should therefore be considered with caution. Conversely, the variation of R_{VV} (q→0)/c with concentration (Figure 3) defines the dilute regime in which supramolecular assemblies free of mutual interactions should be investigated. Consistently, the two different regimes are well documented by the concentration dependence of the translation diffusion coefficient(s) in Figure S4.

We seek also for information on the dynamic properties of these assemblies to reduce ambiguities in the structural characterization of complex systems. **Figure 4** is an example of such information source including the form factor (static) and transport coefficients (dynamic) for the self-assembly of **1** in a dilute aqueous solution. Both translational $C_{VV}(q,t)$ and orientation $C_{or}(q,t)$ relaxation functions are described by a single decay process ascribed to a single population of supramolecular assemblies whose average dimension can be still captured by the longest probing wavelength, as seen by the intensity downturn in the Holtzer presentation, $qR_{vv}(q)/c$ versus q (inset to Figure 4).[22] Moreover, the limiting value of orientation relaxation rate Γ_r at q = 0 is nonzero (upper inset) that allows the determination of the rotational diffusion $D_r = \Gamma_r$ (q = 0)/6 in addition to the translation diffusion $D = \Gamma(q)/q^2$ at q = 0.[23] We should note that at this extremely low concentration other scattering (X-ray or neutron) techniques are hardly applicable and $C_{or}(q,t)$ is still measurable owing to the optical anisotropy of the phenyl rings in the parent **1** and **2** structures.

Since the relaxation function $C_{VV}(q,t)$ is unimodal, there is a single contribution to the static $R_{vv}(q)$ which at such dilute conditions is safely obtained from the total intensity and the short amplitude of $C_{VV}(q,t)$. The pattern of $R_{vv}(q)$ is represented well by a worm-like shape[23–25] using an average contour length L ~ 3 μm and Kuhn segment l_K ~ 75 nm (solid line in the Holtzer plot of Figure 4). Further, since the thickness, d, of the chain is ignored, the applicability of this model in the light scattering experiment presumes thin enough (qd>>1) structures; this assumption is justified by the representation of the two diffusion coefficients in Figure S5. The large contour length implies large aggregation number N_S, already suggested by the high molecular weight value ($1.3\cdot10^8$g mol^{-1}) of the supramolecular structures suggesting ~$6\cdot10^4$ **1**-monomers per assembly. Consistency between this number and the value of the contour length (L) implies a micellar structure of the "repeat" unit.

Complementary information on the internal structure of the supramolecular assembly stems from the length density $M/L = qRvv(q)/(\pi Hc)$ ~$6\cdot10^{11}$ g mol^{-1} cm^{-1} obtained from the quasi-plateau qRvv(q)/c value at high q's (inset to Figure 4). For comparison, this quantity for the "monomer" **1** is about $3.8\cdot10^8$ g mol^{-1} cm^{-1} using 2300 g mol^{-1} for its molecular mass and 0.6 nm for its thickness.[26] Hence its repeat unit should contain approximately 16 monomer units.

As already mentioned, uncertainties of the dynamic parameters in the determination of self-assembled structures are minimized if a consistent representation of the dynamic parameters is also obtained. Both transport coefficients, D_0 and D_r can be represented by a worm-like model[23,27] with three adjustable parameters, L_w, Kuhn segment, l_k (l_k = 2 l_p, the persistence length), and thickness, d assuming stick hydrodynamic boundary conditions. The speed-up of the two transport coefficients with flexibility L/l_p for constant contour length L_w and d, and their expected slowdown, though with different rate, with increasing L and d is shown (Figure S5). A simultaneous representation of both D_0 and D_r (skew and vertically hatched boxes in Figure S5) of the **1** assembly occurs for L_w ~ 2.2 μm, L/l_p ~70, d ~30 nm, i.e., l_p ~ 30 nm in agreement with the representation of the $R_{vv}(q)$ pattern in Figure 4. Considering the presence of size polydispersity[28,29] and the different moments of the distribution entering the static and dynamic experiments, the dimensions and conformation of the supramolecular structure in dilute aqueous solutions of **1** can be adequately estimated.

Turning to the structure characterization for **2**, the experimental situation is less convenient due to the lack of access

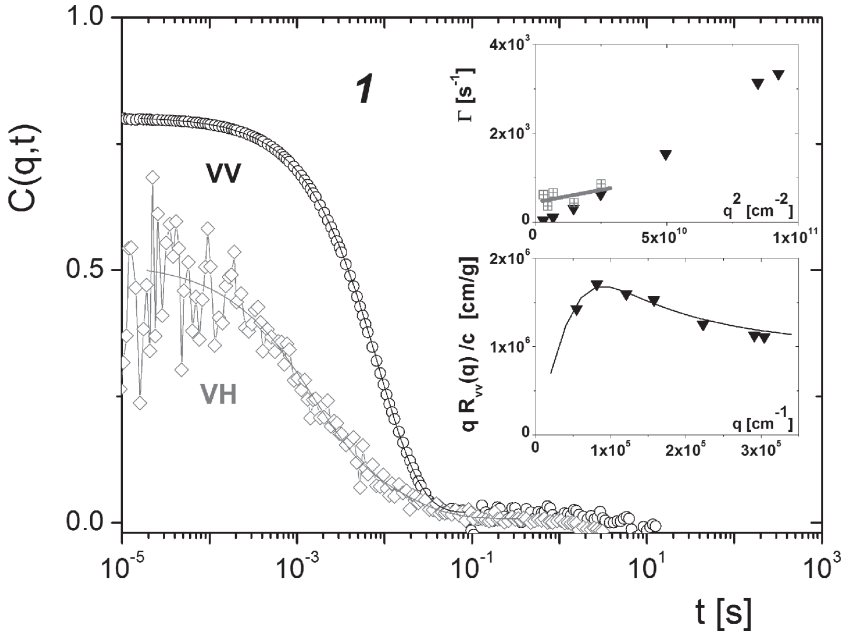

Figure 4. Normalized field correlation functions $C_{vv}(q,t)$ (open circles) for the translational diffusion dynamics and $C_{or}(q,t)$ (open rhombi) for the orientation dynamics at a scattering wave vector q = 0.0081 nm^{-1} and 20 °C for **1** at 0.007 g L^{-1} recorded after annealing at T = 50 °C for few hours and subsequent slow cooling to 20 °C. Inset: The single translational and rotational relaxation rate, and the Holtzer plot $qR_{vv}(q)$ vs q. Solid line denotes the representation by a worm-like model with a persistence length l_k = 65 ± 10 nm.

Structural parameters	1	2
M_w [g mol^{-1}]	1.3×10^8	1.8×10^9
M/L [g mol^{-1} cm^{-1}]	6×10^{11}	7×10^{12}
L_w [μm]	2.25	6.0
L/ l_p	70	150

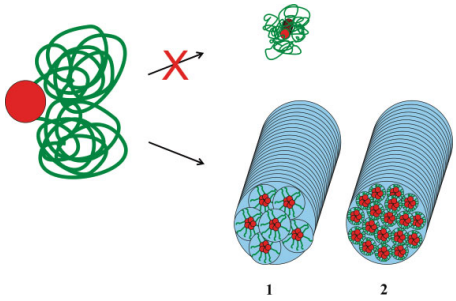

Figure 5. Structural parameters for **1** and **2** self-assembled structures in aqueous solution obtained from dynamic and static experiment. Schematic representation of the proposed self-assembled equilibrium structures of **1** and **2** conforming to the structural parameters of the table.

to all previous physical quantities. Figure S6, the analogue of Figure 4 for **1**, shows that at the concentration of 2.5 10^{-4} g L^{-1} the assemblies are too large to be captured by the longest light scattering wavelength, i.e., absence of downturn in the Holtzer plot. Consistently, the rotational D_r is too low, i.e., the intercept Γ_r (q = 0) is not finite (insets to Figure S6). The information is then limited to the translation coefficient D_0 and the length density M/L = $qR_{vv}(q)/(\pi Hc)$ ~$7 \cdot 10^{12}$ g mol^{-1} cm^{-1} obtained from the quasi-plateau $qR_{vv}(q)/c$ value at high q's in Figure S6 which clearly exceeds the corresponding plateau in Figure 4. The large *M/L* along with the shape of the Holtzer plot suggests high molecular mass. A rough estimate of the latter can be obtained from the R_{VV} (q→0)/c obtained from the intercept in the Debye plot which predicts linear dependence of $[R_{VV}$ (q→0)$]^{1/2}$ versus q^2 at low q's; $M_w = R_{VV}$ (q→0)/Hc is about 10 times higher than for **1**. The description of D_0 and D_r~0 (skew and vertically red hatched boxes in Figure S5) by the worm-like model suggests larger dimensions: L ~ 6.0 µm, L/l_p ~150, d ~30 nm, i.e., l_p ~ 40 nm which implies similar worm-like structure as for the self-assembly of **1.**

The characteristic lengths summarized in the table of **Figure 5** support the proposed supramolecular structures of **1** and **2** in dilute aqueous solutions as schematically illustrated in the same Figure. As the diameter of the worm-like structures of **1** largely exceeds the fully extended molecular size (8.9 nm and 5.1 nm for **1** and **2** according to to Corey-Pauling-Koltun model) a columnar structure with a single molecule per layer, in which PEG protects the hydrophobic core can be excluded. In fact, each layer contains large number of molecules accounting for the high *M/L* values, which is different for the two structures. According to the hydrophilic/hydrophobic interactions and Percec's tobacco mosaic virus model the HPB-PEG derivatives can self-assemble to small fibers.[7,8]

Further, we assume that several fibers are bundled to a single large supermolecular object (Figure 5) confirmed by cryo-TEM at high concentration (Figure 2). Superstructures of bundled fibers were reported for amphiphilic block copolymers of oligo(phenylene vinylene) and poly(propylene oxide).[13]

The assemblies of **2** have a higher density than **1**. In **2**, the shorter PEG chains can accommodate more molecules in the same cross-section. Based on the table in Figure 5, the superstructures of **1** and **2** with a volume V = $\pi d^2 L/4$ and mass M_w/N_A (N_A is the Avogadro number) have a density of about 0.2 g·cm^3 and 0.7 g·cm^3 for **1** and **2,** respectively. This disparity can be rationalized by the difference in swelling of short and long (degree of polymerization N>12) PEG chains in water.[30] It is already reported in literature that the thickness and swelling behavior from monolayers of PEG chains are strongly dependent on the length of the PEG chains. For example, an increase of the degree of polymerization of the PEG chains from 3 to 15 leads to structural changes and the nature of the PEG chains changes from dense packing to a swollen state. We assume a similar behavior for our fibers formed by the molecule **1** or **2**. These amphiphiles can be considered core-shell systems in which the core is formed by HPB and the shell by PEG. Supported by the results obtained for layers, we deduce that the PEG shell of an isolated fiber of **1**, which has arms with a polymerization degree of 17, is more swollen than the shell of a fiber of **2** having only 8 ethylene glycol units per arm. This denser packing in the PEG shell observed for molecule **2** is further enhanced by the doubling of the number of PEG chains per building block from **1** to **2** (illustrated in Figure 5).

Comparing the overall diameter of the bundles of **1** and **2**, the diameter is in both cases 30 nm and therefore independent of the shape of the molecule and the PEG chain length. Surprisingly, the persistence length of the supramolecular structures appears to be virtually unaffected by the number of molecules per layer (much higher for **2**) which do, however, affect the overall fiber length. Therefore, we conclude that the persistence length is controlled less by the PEG chains than by the columnar stacking of HPB (Figure 5).

In conclusion, HPB-PEG derivatives form bundles of hydrogel fibers in very dilute aqueous solution. Remarkably, the water amount in the hydrogel fibers does not depend on the number of hydrophilic groups but on the length of the PEG chains and the substitution pattern of the precursor molecules. Molecule **2** with the shorter PEG chains led to longer self-assembled structures containing less water than the fibers formed by the longer PEG chains. We assume that the denser packing of the four PEG chains in **2** hampers the water uptake, while **1** has only two PEG arms that can easily swell in an aqueous phase. The hydrogel fibers with the variable water uptake resemble nature systems unlike fiber formation processes e.g., extruding, microfluidic processes, and electrospinning. Similar to natural systems, antagonistic forces (hydrogen bonds, van der Waals forces) are responsible

NANO MICRO small

for the formation of well-defined objects. It is demonstrated that in water swellable fibers can be created utilizing hydrophobic and hydrophilic interactions. These interactions have to be carefully tuned to allow for a thermodynamic control which we showed by the comparison between amphiphiles containing HPB and HBC as hydrophobic building blocks. Due to the strong interaction among the HBC units the yielded self-assembly becomes kinetically controlled as only undefined aggregates are obtained by TEM. Herein, we demonstrate an analogue to the fiber formation process in nature by using a self-assembly process to yield hydrogel fibers. Similar to nature, our case was controlled by different molecular interactions. However, the main difference is that nature achieves such extended hydrogel fibers by the self-assembly of large polymers such as polycarbohydrates or polypeptides, while we focused on "small" two-dimensional amphiphiles.

Supporting Information

Supporting Information is available from the Wiley Online Library or from the author.

Acknowledgements

The authors acknowledge financial support from the European Commission under the Seventh Framework Program by means of the grant agreement for the Integrated Infrastructure Initiative N. 262348 European Soft Matter Infrastructure (ESMI) and GSRT in the framework of the program THALIS(Metaassembly). The authors thank the Stiftung Stipendien-Fonds des Verbandes der Chemischen Industrie e.V. for funding.

[1] S. Nomura, A. Hiltner, J. B. Lando, E. Baer, *Biopolymers* **1977**, *16*, 231–246.
[2] E. L. Bakota, O. Sensoy, B. Ozgur, M. Sayar, J. D. Hartgerink, *Biomacromolecules* **2013**, *14*, 1370–1378.
[3] S. Zhang, *Biotechnol. Adv.* **2002**, *20*, 321–339.
[4] F. Jianqi, G. Lixia, *Eur. Polym. J.* **2002**, *38*, 1653–1658.
[5] H. Onoe, R. Gojo, K. Kuribayashi-Shigetomi, S. Takeuchi, in 25th IEEE International Conference on Micro Electro Mechanical Systems (MEMS) **2012**, pp. 1065–1068.
[6] A. Hsieh, T. Zahir, Y. Lapitsky, B. Amsden, W. Wan, M. S. Shoichet, *Soft Matter* **2010**, *6*, 2227–2237.
[7] S. D. Hudson, H.-T. Jung, V. Percec, W.-D. Cho, G. Johansson, G. Ungar, V. S. K. Balagurusami, *Science* **1997**, *278*, 449–452.
[8] V. Percec, J. Heck, G. Johansson, D. Tomazos, *Macromol. Symp.* **1994**, *77*, 237–265.
[9] J. N. Israelachvili, *Intermolecular and Surface Forces* **1991**, 291–292.
[10] T. Aida, E. W. Meijer, S. I. Stupp, *Science* **2012**, *335*, 813–817.
[11] P. Y. W. Dankers, T. M. Hermans, T. W. Baughman, Y. Kamikawa, R. E. Kieltyka, M. M. C. Bastings, H. M. Janssen, N. A. J. M. Sommerdijk, A. Larsen, Marja J. A. van Luyn, A. W. Bosman, E. R. Popa, G. Fytas, E. W. Meijer, *Adv. Mater.* **2012**, *24*, 2703–2709.
[12] J. Fei, Z. Zhang, L. Zhong, L. Gu, *J. Appl. Polym. Sci.* **2002**, *85*, 2423–2430.
[13] H. Wang, W. You, P. Jiang, L. Yu, H. H. Wang, *Chem. Eur. J.* **2004**, *10*, 986–993.
[14] M. Muthukumar, C. K. Ober, E. L. Thomas, *Science* **1997**, *277*, 1225–1232.
[15] G. Riess, *Prog. Polym. Sci.* **2003**, *28*, 1107–1170.
[16] L.-I. Atanase, G. Riess, *Polym. Int.* **2011**, *60*, 1563–1573.
[17] L. Schmidt-Mende, A. Fechtenkötter, K. Müllen, E. Moons, R. H. Friend, J. D. MacKenzie, *Science* **2001**, *293*, 1119–1122.
[18] M. Johnsson, P. Hansson, K. Edwards, *J. Phys. Chem. B* **2001**, *105*, 8420–8430.
[19] B. Jönsson, B. Lindman, K. Holmberg, B. Kronberg, Surfactants and Polymers in Aqueous Solution, Wiley: New York **1998**, 255.
[20] H. Kölbel, P. Kurzendörfer, Konstitution und Eigenschaften von Tensiden. Fortschritte der chemischen Forschung Bd. 12, 2, **1969**, Springer Verlag, Berlin.
[21] M. Bockstaller, W. Koehler, G. Wegner, G. Fytas, *Macromolecules* **2001**, *34*, 6353–5358.
[22] A. Holtzer, *J. Polym. Sci.* **1955**, *17*, 432–434.
[23] A. Kroeger, J. Belack, A. Larsen, G. Fytas, G. Wegner, *Macromolecules* **2006**, *39*, 7098–7106.
[24] R. J. Koyama, *J. Phys. Soc. Jpn.* **1973**, *34*, 1029–1038.
[25] A. Kroeger, V. Deimende, J. Belack, I. Lieberwirth, G. Fytas, G. Wegner, *Macromolecules* **2007**, *40*, 105–115.
[26] a) L. Jiménez-García, A. Kaltbeitzel, W. Pisula, J. S. Gutmann, M. Klapper, K Müllen, *Angew. Chem.* **2009**, *121*, 10135–10138; b) J. García, A. Kaltbeitzel, W. Pisula, J. S. Gutmann, M. Klapper, K. Müllen, *Angew. Chem. Int. Ed.* **2009**, *48*, 9951–9953.
[27] H. Yamakawa, M. Fujii, *Macromolecules* **1973**, *6*, 407–415.
[28] S. Bantle, M. Schmidt, W. Burchard, *Macromolecules* **1982**, *15*, 1604–1609.
[29] S. R. Aragon, R. Pecora, *J. Chem. Phys.* **1976**, *64*, 2395–2404.
[30] G. Mathe, C. Gege, K. R. Neumaier, R. R. Schmidt, E. Sackmann, *Langmuir* **2000**, *16*, 3835–3845.

Received: August 30, 2013
Revised: December 6, 2013
Published online: February 25, 2014

